

DOI: 10.1002/cmdc.201200561

A Concise Synthesis of Pyrazole Analogues of Combretastatin A1 as Potent Anti-Tubulin Agents

Roberta Zaninetti, Salvatore V. Cortese, Silvio Aprile, Alberto Massarotti, Pier Luigi Canonico, Giovanni Sorba, Giorgio Grosa, Armando A. Genazzani, and Tracey Pirali*^[a]

Combretastatin A1 (CA1) binds to the β -subunit at the colchicine binding site of tubulin and inhibits polymerization. As such, it is both an antitumor agent and a vascular disrupting agent. It has been shown to be at least tenfold more potent than combretastatin A4 (CA4) in terms of vascular shutdown, which correlates with its metabolism to reactive *ortho*-quinone species that are assumed to be directly cytotoxic in tumor cells. A series of 3,4-diarylpyrazoles were concisely synthesized, one of which, 3-methoxy-6-[4-(3,4,5-trimethoxyphenyl)-1H-pyrazol-3-yl]benzene-1,2-diol (**27**), proved to be a cytotoxic anti-

tubulin agent with low nanomolar potency. We also report that combretastatins, including CA1, CA4, and **27**, are effective against mesothelioma cell lines and therefore have significant clinical promise. Metabolism experiments demonstrate that **27** retains the ability to form *ortho*-quinone species, while the pyrazole ring shows high metabolic stability, suggesting that this compound might result in better pharmacokinetic profiles than CA1, with similar pharmacodynamic properties and clinical potential.

Introduction

Solid tumors require a functional blood supply for growth, making tumor vasculature an attractive target for anticancer therapy. Small molecule vascular disrupting agents (VDAs) cause rapid and selective shutdown of the blood vessels of tumors, which in turn acts to starve the tumor of oxygen and nutrients, resulting in extensive tumor cell necrosis. They differ conceptually from anti-angiogenic agents, which prevent new blood vessel formation from existing vessels. VDAs are more effective in the interior of the tumor, while angiogenesis inhibitors are most effective in the periphery.^[1] Indeed, despite the induction of significant tumor necrosis, a hallmark observation following treatment with VDAs is a "viable rim" of tumor cells observed to survive by receiving nutritional support from the surrounding normal tissue vasculature. Such a viable region of cells can rapidly proliferate and contribute to the eventual regrowth and revascularization of the necrotic tumor center, although the cells remain highly sensitive to additional chemotherapy. As a result, VDAs alone are unlikely to be curative and are being evaluated in combination with conventional anticancer therapies.

Several small molecule VDAs are currently in clinical trials, including the combretastatins (Figure 1, CA4, **1**; CA1, **3**). Originally isolated from the bark of the South African *Combretum caff-*

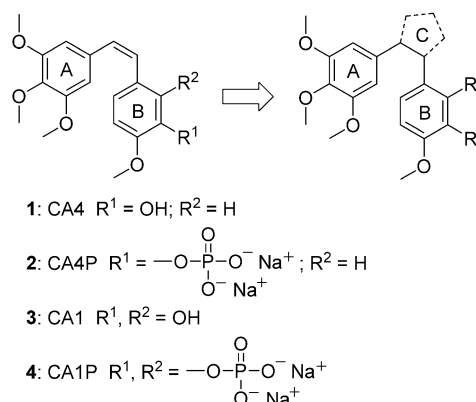


Figure 1. Rigidified analogues of combretastatins A4 and A1.

rum tree,^[2] combretastatins are microtubule-destabilizing agents^[3] that reversibly bind to the β -subunit at the colchicine binding site of tubulin and inhibit tubulin polymerization.^[4] This leads to both vascular-mediated effects and to a direct effect on tumor cell viability. The water-soluble prodrug CA4P (Figure 1, **2**, fosbretabulin, Zybrestat) has undergone extensive Phase II clinical evaluation^[5] in combination with conventional chemotherapy and radiotherapy against a range of tumor types. The entrance of **2** into clinical trials has spurred the development of second-generation VDAs, such as CA1P (Figure 1, **4**, OXi4503), which has recently completed Phase I clinical trials in patients with advanced solid tumors.^[6] Although CA1P is a close analogue of CA4, the extra hydroxy group on ring B (Figure 1) is clearly influential in the antitumor profile of the compound. CA1P proved to be more potent than CA4 in pre-clinical models in terms of vascular shutdown,^[7] and compara-

[a] Dr. R. Zaninetti, S. V. Cortese, Dr. S. Aprile, Dr. A. Massarotti, Prof. P. L. Canonico, Prof. G. Sorba, Prof. G. Grosa, Prof. A. A. Genazzani, Dr. T. Pirali

Dipartimento di Scienze del Farmaco
Università degli Studi del Piemonte Orientale "A. Avogadro"
L.go Donegani 2, 28100 Novara (Italy)
E-mail: tracey.pirali@pharm.unipmn.it

Supporting information for this article is available on the WWW under <http://dx.doi.org/10.1002/cmdc.201200561>.

tive studies indicate that the "viable rim" surviving after treatment with this agent is significantly smaller than that observed for CA4.^[8] It has been speculated that the increased antitumor efficacy may be due to the metabolism of CA1 to reactive *ortho*-quinone species that are assumed to be cytotoxic in tumor cells as they can bind to cellular nucleophiles and also produce free radicals leading to the enhancement of oxidative stress.^[9]

Structure–activity relationship (SAR) studies have demonstrated that a 3,4,5-trimethoxy substituted ring A and a 4-methoxysubstituted ring B, separated by a double bond with *cis* configuration, are crucial for the anti-tubulin activity of combretastatins (Figure 1).^[10] On the other hand, isomerization to the less active *trans* isomer and the metabolic instability of the olefinic bridge may compromise the development of combretastatins as drug candidates. Replacing the stilbene core with a central heterocyclic ring is the main strategy used to lock the molecule into the *cis* orientation while preventing undesirable metabolic reactions. In addition to better stability, *cis*-restricted analogues can lead to increased polarity and different pharmacodynamic properties, with higher potency and selectivity than the parent combretastatin.

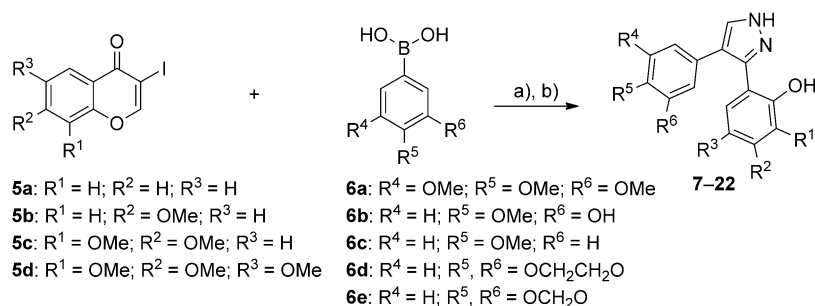
As part of our ongoing program regarding the synthesis of novel active compounds through the use of multicomponent reactions, we were intrigued by the possibility of exploiting a one-pot synthesis^[11] to generate novel 3,4-diaryl pyrazole analogues of CA1. Indeed, we realized that this known methodology was perfectly suited for the preparation of derivatives of CA1, as it results in the formation of the requisite free phenol.

Pyrazole-based heterocycles are not new in the arena of rigidified combretastatin analogues, especially among CA4 derivatives. Lee and co-workers described a series of 3,5-diaryl pyrazoles that display low cytotoxicity in tumor cell lines due to their planar conformation.^[12] On the other hand, two 3,4-diaryl pyrazoles were reported by Ohsumi and collaborators, one of which showed marked anti-tubulin activity and cytotoxicity.^[13] This favorable biological profile encouraged us toward the synthesis and evaluation of 3,4-diaryl pyrazoles as CA1 analogues.

Results and Discussion

Chemistry

A series of 3,4-diaryl pyrazoles were synthesized by means of a convenient one-pot, three-component process (Scheme 1). The first step of the process was a Suzuki coupling between 3-iodochromone **5a–d** and boronic acid **6a–e** in the presence of Pd(PPh₃)₄.^[14] After completion of the reaction, aqueous hydrazine was added to the reaction mixture, leading to 3,4-diaryl



Scheme 1. Synthesis of combretapyrazoles **7–22** by a three-component reaction. Reagents and conditions: a) K₂CO₃, Pd(PPh₃)₄, THF, H₂O, reflux, 4–24 h; b) NH₂NH₂ solution (35% w/w in H₂O), reflux, 12–36 h (40–80% over two steps).

pyrazoles **7–22**.^[15] As postulated,^[15a] hydrazine undergoes initial 1,4-conjugate addition to the double bond of the 3-arylchromone with subsequent ring opening, followed by attack of the unsubstituted hydrazine nitrogen to the carbonyl group and cyclization. This one-pot process resulted in the formation of *o*-hydroxyphenylpyrazoles **7–22**, providing facile construction of these heterocycles as CA1 analogues.

3-Iodochromones **5a–d** were easily prepared through Gamill's protocol, based on the condensation of the corresponding 2-hydroxyacetophenone with dimethylformamide-dimethylacetal, leading to the enamine that is directly subjected to iodination cyclization (see Supporting Information).^[16]

By combining four different chromones **5a–d** and five boronic acids **6a–e**, the first series of 16 pyrazoles was synthesized (Table 1). In all cases, the process worked under mild reaction conditions and in short times, giving moderate to good overall yields (40–80%). These derivatives are all new synthetic compounds with the exception of **8**,^[11] **9**,^[17] **12**,^[15a] and **13**;^[18] how-

Table 1. Synthesized combretapyrazoles **7–22**.

Compd	R ¹	R ²	R ³	R ⁴	R ⁵	R ⁶	Yield [%]
7	H	H	H	OMe	OMe	OMe	80
8	H	H	H	H	OMe	H	51
9	H	H	H	OCH ₂ CH ₂ O	H	H	46
10	H	OMe	H	OMe	OMe	OMe	51
11	H	OMe	H	OH	OMe	H	66
12	H	OMe	H	H	OMe	H	63
13	H	OMe	H	OCH ₂ CH ₂ O	H	H	53
14	H	OMe	H	OCH ₂ O	H	H	48
15	OMe	OMe	H	OMe	OMe	OMe	67
16	OMe	OMe	H	OH	OMe	H	40
17	OMe	OMe	H	H	OMe	H	61
18	OMe	OMe	H	OCH ₂ CH ₂ O	H	H	56
19	OMe	OMe	H	OCH ₂ O	H	H	63
20	OMe	OMe	OMe	OMe	OMe	OMe	45
21	OMe	OMe	OMe	OH	OMe	H	69
22	OMe	OMe	OMe	H	OMe	H	53

ever, it must be stressed that this is the first report on the cytotoxic and anti-tubulin activity of these pyrazole derivatives.

As the preparation of the requisite 8-hydroxy-3-iodo-7-methoxy-4*H*-chromen-4-one was not accomplished, a different strategy was used for the synthesis of pyrazoles **27–29** (Scheme 2). This failure is presumably due to interference by the additional nucleophilic phenol group with the iodination cyclization, supported by the absence of such reactions involving 2,3-dihydroxyacetophenones reported in the literature.

The alternative protocol consists of three steps. Intermediates **25a–c** were prepared from 3-methoxycatechol **23** and phenylacetic acids **24a–c** by regioselective Friedel–Crafts acylation in the presence of boron trifluoride etherate as a solvent and Lewis acid. The cyclization reaction was carried out with *N,N*-dimethylformamide–dimethylacetal, and the resulting 3-arylchromones **26a–c** were then condensed with hydrazine to give the final pyrazoles **27–29**.

As compound **27** proved to be the most potent of the synthesized pyrazoles (see *Biological evaluation* below), we decided to explore the heterocyclic ring by varying the hydrazine component. Arylchromone **26a** was condensed with *N*-methylhydrazine (Scheme 3). The reaction proved to be selective and afforded *N*-methyl pyrazole **30** as the major product. The structure was assigned on the basis of ¹H NMR, in which the phenolic proton that forms the intramolecular hydrogen bond with the pyrazole nitrogen is shifted downfield, with a signal at $\delta = 10.86$ ppm. This result can be explained by initial addition of the more nucleophilic methyl-substituted hydrazine nitrogen to the double bond of chromone.

Finally, we also decided to investigate whether this strategy could be employed for the synthesis of 4,5-diaryl isoxazoles. To this end, hydroxylamine was used as the nucleophile, and the isoxazole **31** was synthesized in 64% yield (Scheme 3).

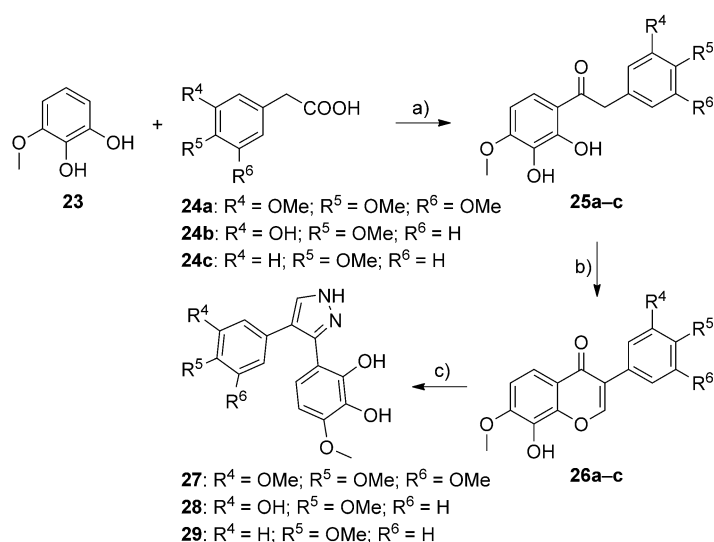
Biological evaluation

To investigate the activity of the synthesized compounds, we employed a neuroblastoma cell line (SH-SY5Y), which we have previously shown to be sensitive to combretastatins. We first tested all compounds at a concentration of 10 μM (Table 2) for 64 h. All analogues that were able to induce cytotoxicity at this concentration (a decrease in viability to at least 30% of control) were carried forward, and a full dose–response was performed, treating cells for 48 h. In this set of experiments, CA4 (**1**) and CA1 (**3**) displayed similar IC_{50} values for cytotoxicity (2.6 ± 1.1 and 1.3 ± 1.2 nM, respectively). Compounds **15**, **21**, **22**, and **27** had IC_{50} values in the nanomolar range, and, as expected, all contain a 3,4,5-trimethoxysubstituted ring A and a 4-methoxysubstituted ring B, supporting the previous findings that this is the optimum substitution pattern for combretastatins.^[10]

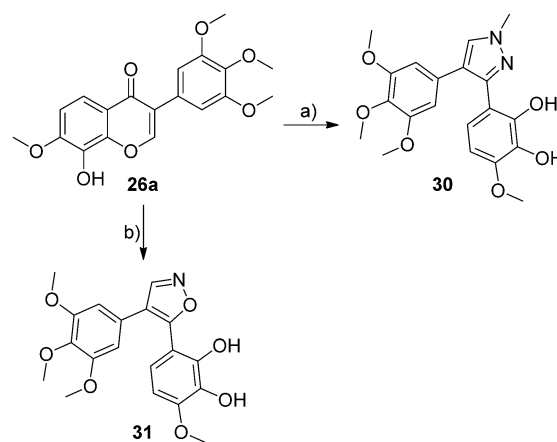
Two of the synthesized pyrazole-bearing analogues displayed considerable potency, with **27** and **15** displaying IC_{50} values of 5.4 ± 1.1 and 12.0 ± 1.0 nM, respectively (Table 2; see

the Supporting Information for concentration–response curves of compounds **1**, **3**, **15**, and **27**). Compound **27** is the rigidified analogue of CA1, while **15** has a methoxy group in position 3 on ring B instead of a hydroxy moiety. Interestingly, no activity was observed for the *N*-methylated analogue of **27** and **30**.

We therefore decided to carry compounds **15** and **27** forward for further characterization. Tubulin inhibitors are characterized by their ability to arrest cells in the G_2/M phase of the cell cycle. We therefore treated SH-SY5Y cells for 24 h with compounds at concentrations three times the IC_{50} values (a protocol which we previously validated)^[19] and performed cell-cycle analysis with propidium iodide staining. Both compounds were as effective as **3** at increasing the percentage of cells in the G_2/M phase (Figure 2).



Scheme 2. Synthesis of combretapyrazoles **28–30** by a three-step sequence. *Reagents and conditions:* a) *p*-TsOH, BF₃·Et₂O, 85 °C, 90 min, **a**: 30%, **b**: 52%, **c**: 22%; b) DMF–DMA, 90 °C, 30 min, **a**: 88%, **b**: 69%, **c**: 90%; c) NH₂NH₂ solution (35% w/w in H₂O), THF, reflux, 3 h, **27**: 63%, **28**: 51%, **29**: 53%.



Scheme 3. Synthesis of combretapyrazole **30** and combretaisoxazole **31**. *Reagents and conditions:* a) methylhydrazine, THF, reflux, 3 h, 50%; b) NH₂OH·HCl, Py, EtOH, 65 °C, 2 h, 64%.

Table 2. Cytotoxicity in SH-SY5Y cells and predicted binding energy of the synthesized compounds.			
Compd	Viability [%] ^[a]	IC ₅₀ [nM] ^[b]	Chemgauss4 ^[c]
1	36.7 ± 4.2	2.6 ± 1.1	-13.235
3	31.4 ± 0.7	1.3 ± 1.2	-14.815
7	75.1 ± 2.9	NA	NA
8	92.7 ± 0.3	NA	NA
9	88.9 ± 1.0	NA	NA
10	21.6 ± 0.8	> 1000	NA
11	39.8 ± 1.0	> 1000	NA
12	69.9 ± 0.6	NA	NA
13	46.9 ± 3.0	> 1000	NA
14	59.9 ± 1.7	> 1000	NA
15	11.7 ± 1.2	12.0 ± 1.0	-10.768
16	36.2 ± 0.6	> 1000	NA
17	91.5 ± 3.8	NA	NA
18	48.6 ± 2.1	> 1000	NA
19	82.7 ± 5.4	NA	NA
20	39.4 ± 0.5	> 1000	NA
21	27.0 ± 0.7	61.0 ± 1.2	-12.730
22	41.9 ± 1.5	332.9 ± 1.2	-12.811
27	35.7 ± 1.4	5.4 ± 1.1	-13.945
28	99.1 ± 3.2	NA	NA
29	66.8 ± 1.5	> 1000	NA
30	80.9 ± 2.5	NA	-12.394
31	20.4 ± 0.9	6.4 ± 1.1	-14.688

[a] Cell viability was determined at 10 μM and is expressed as the percentage of control; data represent the mean ± SEM of two experiments. [b] IC₅₀ values were determined using GraphPad Prism software; data represent the mean ± SEM of at least nine determinations from three separate experiments; NA: data not available. [c] The Chemgauss4 score was generated using FRED software to rank compounds that exhibited tubulin inhibition properties; NA: data not available.

Lastly, to assure ourselves that tubulin was the protein target of these compounds, we performed a tubulin polymerization assay. Briefly, cells were treated with the selected compounds for 24 h, then tubulin was extracted in the presence of paclitaxel. As expected, **3**, **15**, and **27** were all able to increase the proportion of soluble tubulin over the amount polymerized (Figure 3). In conclusion, therefore, compounds **15** and **27** are *in vitro* cytotoxic anti-tubulin agents with low nanomolar potency.

While our characterization was centered on neuroblastoma cells, we also tested these agents on mesothelioma in light of a recent study using this class of drugs in Phase I/II trials against this tumor type.^[20] Indeed, this is a disease with a very poor prognosis in which chemotherapy has not been able to significantly affect the course of the disease.^[21] We therefore tested **1**, **3**, **15**, and **27** on two separate mesothelioma cell lines, REN (which has an epithelioid phenotype)^[22] and MSTO-211H (a more aggressive biphasic phenotype).^[23] Surprisingly, CA1, CA4, and the rigidified combretastatins synthesized by us were effective against this tumor type. The epithelioid phenotype was more sensitive, and the IC₅₀ values of these compounds were similar to those obtained for neuroblastoma (For **1**, **3**, **15**, and **27**, IC₅₀ values in REN cells are 3.1 ± 1.1, 1.4 ± 1.1, 19.3 ± 1.1, and 10.5 ± 1.0 nM, respectively; in MSTO-211H cells: 2.7 ± 1.4, 1.2 ± 1.1, 21.0 ± 1.2, and 5.4 ± 1.1 nM, respectively) (Figure 4). Notably, for the MSTO-211H line, only ~40% of cells

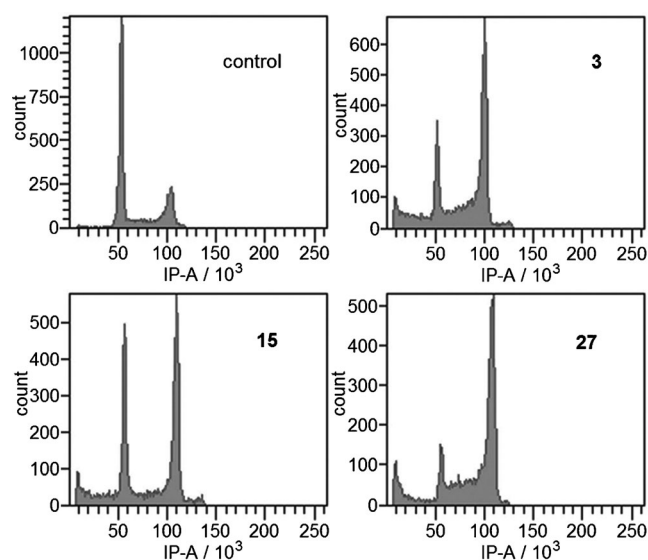


Figure 2. Cell-cycle analysis of SH-SY5Y neuroblastoma cells treated for 24 h with vehicle (control) or 3 × IC₅₀ values of the indicated compounds. Data are representative of three separate experiments; y-axes represent cell number, and x-axes represent fluorescence on a linear scale. See the Supporting Information for details regarding quantitative analysis of the different populations.

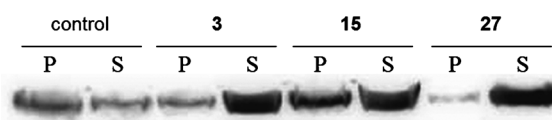


Figure 3. Western blot of α-tubulin extracted in the presence of paclitaxel from SH-SY5Y cells treated with the indicated compounds at 3 × IC₅₀ values for 24 h. P represents the pelleted fraction (polymerized tubulin), and S represents the soluble fraction (unpolymerized tubulin).

were sensitive to our compounds, even at the higher concentrations tested. Finally, cell-cycle analysis confirmed that the cytotoxicity of these compounds was related to cell-cycle arrest in G₂/M phase (see Supporting Information).

Capitalizing on the structure–activity relationship information collected for pyrazoles, we synthesized and tested the isoxazole-rigidified analogue of **3** and **31**. Once again, this compound proved to be active, with an IC₅₀ value of 6.4 ± 1.1 nM (Table 2), similar to that reported for the isoxazole analogue of **1**.^[24]

In vitro metabolism

As mentioned previously, it has been postulated that the *in vivo* activity of CA1 is potentiated by its metabolites, the reactive *ortho*-quinone species. To investigate whether compounds **15**, **27**, and **31** could share this mechanism *in vivo*, we incubated these compounds in the presence of rat and human liver subcellular fractions containing all of the hepatic cytochrome P450 enzymes, most of the oxidoreductases, and the main conjugation systems (glucuronosyltransferases and sulfo-

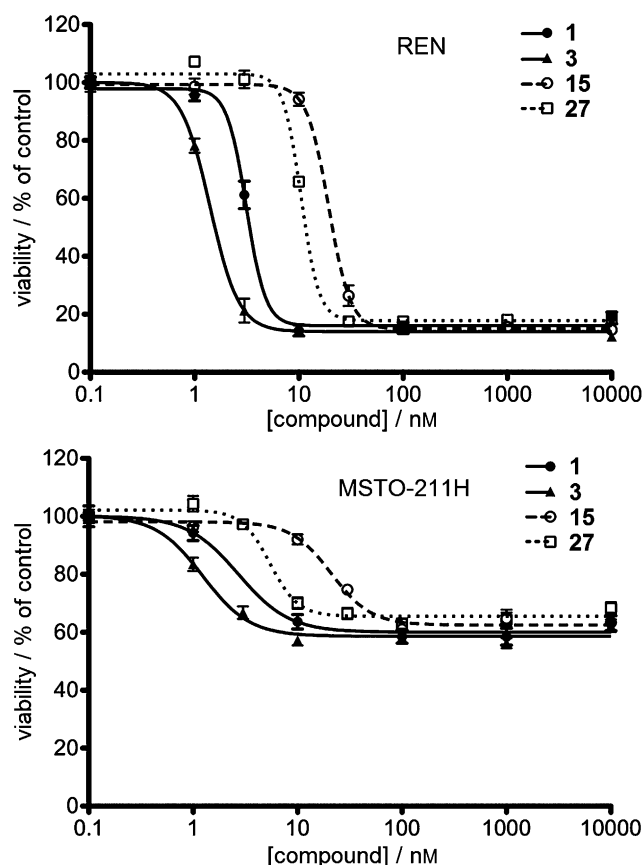


Figure 4. Dose–response curves of CA4 (1), CA1 (3), and the most potent pyrazole analogues of combretastatin A1 (15 and 27) as determined by MTT assay in two mesothelioma cell lines (REN and MSTO-211H). Values represent the mean \pm SEM of at least six determinations from two separate experiments. See text for IC_{50} values.

transferases). In particular, phase I metabolism was performed in microsomal incubations in the presence of a NADPH-regenerating system, allowing us to evaluate the metabolites arising from oxidative metabolic pathways. Phase II metabolism was investigated in microsomes and S9 fractions using the appropriate cofactors to evaluate the formation of glucuronide and sulfate conjugates. Moreover, microsomal incubations were also carried out in the presence of the nucleophilic trapping agent GSH, which is capable of reacting with electrophilic intermediate species.

Even though a systematic study of metabolic fate of CA1 has not been published, the formation of quinone reactive species has been established^[9] and their role in cytotoxicity has also been postulated. Generally, the metabolic fate of combretastatins involves three main metabolic pathways: O-demethylation, aromatic hydroxylation, and glucuronidation. It is worth noting that *Z/E* isomerization of the olefin bond and formation of quinone species could also be observed. Because of their structural similarity to 3, compounds 15, 27, and 31 may share a similar metabolic pattern, although *cis* restriction would prevent *Z/E* isomerization. Indeed, as reported in Table 3, the metabolites arising from both O-demethylation and conjugation were observed in LC–MS–MS chromatograms

Table 3. Metabolic profile for compounds 15, 27, and 31.			
Metabolic Pathway	15	Compd 27	31
<i>Phase I</i>			
O-Demethylation	+	+	+
Aromatic hydroxylation (ring B)	+	–	–
Metabolic activation (quinones)	+	+	+
<i>Phase II</i>			
Glucuronic acid conjugates	+	+	+
Sulfate conjugates	–	+	+

(see Supporting Information) for compounds 15, 27, and 31. Moreover, the formation of *ortho*-quinone species, arising from catechol oxidation, was established for compounds 27 and 31 through identification of their GSH adducts by mass spectrometry. In addition, for compound 15, the formation of a *para*-quinone metabolite was observed; this is only a secondary metabolite arising from oxidation of the corresponding *para*-hydroquinone metabolite. These features suggest that for compounds 27 and 31, the primary *ortho*-quinone metabolites may contribute to pharmacodynamic activity, as suggested for CA1.

Importantly, the pyrazole and isoxazole rings did not undergo metabolic transformation, thereby conferring the expected stability to the combretastatin scaffold. In contrast to zonisamide, which also contains an isoxazole moiety,^[25] the ring of compound 31 appeared stable toward reductive metabolism as assessed in the presence of the cytosolic fraction (Table 3).

From a quantitative point of view, compounds 15 and 27 tested in the phase I rat and human microsomal incubations showed an extent of transformation ranging from ~41 to ~63% (amount of residual substrate after incubation), while a greater range was observed for compound 31 (11–80%). In particular, for compounds 15 and 27, the oxidative microsomal transformations encompass both O-demethylation and the formation of *ortho*-quinone metabolites. As previously reported for 1 and 3,^[26] the glucuronidation pathway plays a relevant role in metabolism (Table 4); the percentage of transformation for compounds 15, 27, and 31 ranged from 2–79%, with the isoxazole derivative being the least stable and 27 the most stable.

Table 4. Metabolic stability of compounds 15, 27, and 31. ^[a]							
Compd	Phase I			Phase II Glucuronides		Phase II Sulfates	
	RLM	HLM	Cytosol _{rat}	RLM	HLM	S9 _{rat}	S9 _{human}
15	55	63	–	23	54	~100	~100
27	41	55	–	59	79	~100	~100
31	11	80	~100	2	3	~100	97

[a] HLM: human liver microsomes, RLM: rat liver microsomes; data are expressed as peak area percent relative to controls (without microsomes) obtained from LC–DAD–UV analyses ($n=2$) of incubation extracts ($t=60$ min).

Molecular modeling

Molecular modeling studies were performed to investigate the potential binding ability of these compounds to the colchicine binding site of α,β -tubulin. The docking score (Chemgauss4) implemented in the FRED software was used to rank the compounds that exhibited tubulin inhibition properties (**15**, **21**, **22**, **27**, and **31**). Unfortunately, there was no evident correlation between scores and IC_{50} values (Table 2). This observation was not unexpected, as scoring of a class of small compounds remains a challenge.^[27]

Different colchicine domain inhibitors were identified to interact in three conserved regions,^[28] and our docking studies showed that the trimethoxyphenyl ring of **3** and its rigid analogues lie in a hydrophobic pocket within zone 2 (Lys β 352,

Asn β 350, Leu β 378, Ala β 316, Leu β 255, Lys β 254, Ala β 250 and Leu β 242), while the other side of the molecule interacts in zone 1 through van der Waals contacts (Val α 181, Ser α 178 and Val β 315). CA1 forms one hydrogen bond between the phenolic group of ring B and the carbonyl group of Thr α 179, and one hydrogen bridge is shown between the methoxy group of ring A and the thiol group of Ser β 241 (Figure 5 a). Surprisingly, none of our compounds were able to create this hydrogen bond interaction. Compounds **15** and **27**, the most active pyrazole analogues, showed additional hydrogen bonding interactions: **15** binds both Thr α 179 and Val α 181 (Figure 5 b), while both hydroxy groups of **27** interact with Thr α 179 (Figure 5 d). The other most active compound, **31**, shows the same pattern of interactions as **27** (Figure 5 f). This model may explain the loss of activity in the case of other less active compounds; for

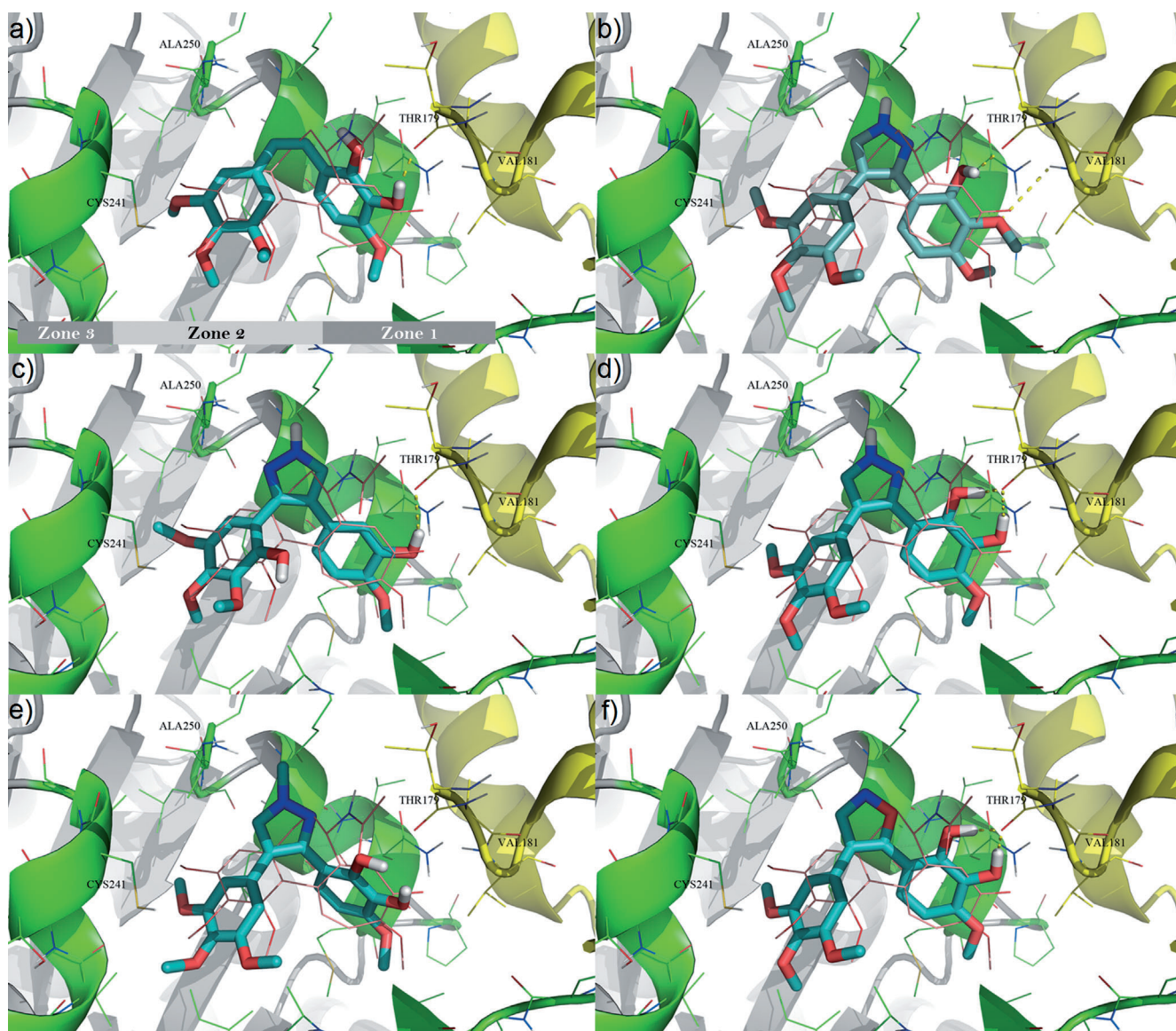


Figure 5. The colchicine domain. The tubulin backbone is shown in ribbon representation (α -tubulin: yellow; β -tubulin: green). Wire model of colchicine (pink) is superimposed. Tubulin residues within 4.0 Å from colchicine are shown as wire models. Hydrogen bonds ($d < 3$ Å) are shown as yellow dotted lines. A schematic representation of interaction zones 1–3 is reported; see ref. [28] for further detail. Docking results for compounds a) **3**, b) **15**, c) **21**, d) **27**, e) **30**, and f) **31** are shown as stick models (carbon atoms in cyan).

example, compound **21** binds with a reverse orientation of the pyrazole ring (Figure 5c), whereas the 2-hydroxy-3,4,5-trimethoxybenzyl ring in zone 2 appears to be poorly tolerated. Furthermore, to understand the absence of anti-tubulin activity of compound **30**, an N-methylated analogue of **27**, we investigated its binding mode (Figure 5e), and docking results showed the absence of contacts in zone 1, while the interaction with α -tubulin is a conserved signature of this class of anti-tubulin agents. Our modeling data, therefore, are compatible with the hypothesis that the synthesized agents act at the colchicine binding site.

Conclusions

In this work, we capitalized on a multicomponent reaction to generate pyrazole- and isoxazole-rigidified compounds of CA1. Among all of the analogues generated, the most potent compounds were closely related to the parent compound, as **27** and **31** are the two rigidified analogues of CA1 and **15** bears a methoxy group at position 3 on ring B instead of a hydroxy moiety.

Compounds **15** and **27** showed activity similar to that of CA1 and CA4 against neuroblastoma in vitro. Importantly, we also show that combretastatins are active in mesothelioma cells. We feel this is an important observation with translational implications. Indeed, we have become aware that a combretastatin analogue has recently entered clinical trials for this tumor type, and our observations would support this indication.^[20]

The actions of CA1 in vivo are thought to be potentiated by one of its reactive metabolites, the *ortho*-quinone. Metabolism experiments show that both **27** and **31** retain the ability to form this species. Furthermore, the pyrazole ring of **27** exhibits higher metabolic stability than CA1, which might suggest that this compound or other compounds stemming from this investigation might result in better pharmacokinetic profiles, with similar pharmacodynamic profiles in the clinic.

Experimental Section

Chemistry

General: Commercially available reagents and solvents were used without further purification. When needed, the reactions were performed in flame- or oven-dried glassware under a positive pressure of dry N_2 . Toluene was purified by distillation over sodium and stored on activated molecular sieves (4 Å), and CH_2Cl_2 was purified by distillation over P_2O_5 and stored on activated molecular sieves (4 Å). Melting points were determined in open glass capillaries with a Stuart scientific SMP3 apparatus and are uncorrected. All compounds were verified by IR (FT-IR Thermo-Nicolet Avatar), 1H and ^{13}C APT (JEOL ECP 300 MHz), and mass spectrometry (Thermo Finnigan LCQ-deca XP-plus) equipped with an ESI source and an ion trap detector. Chemical shifts (δ) are reported in parts per million (ppm). Column chromatography was performed on silica gel (Merck Kieselgel, 70–230 mesh, ASTM). Thin-layer chromatography (TLC) was carried out on 5 cm \times 20 cm plates with a layer thickness of 0.25 mm (Merck silica gel 60 F₂₅₄) and were visualized with $KMnO_4$ as necessary. Purity of the target compounds (> 95%) was

determined via elemental analysis and was within $\pm 0.4\%$ of the calculated value.

General procedure for the synthesis of pyrazoles 7–22: 3-Iodochromone **5** (1 equiv) was dissolved in THF/H₂O (4:1; 7 mL). Boronic acid **6** (1.1 equiv), K_2CO_3 (2 equiv), and $Pd(PPh_3)_4$ (2 mmol) were added to the solution, and the reaction mixture was stirred at reflux and monitored by TLC. After the reaction was completed, aq. NH_2NH_2 (35% w/w; 2 equiv) was added, and the reaction mixture was heated at reflux with stirring until completion. The solvent was concentrated in vacuo, and the crude residue was diluted with EtOAc/H₂O (50 mL). The organic layer was washed with H₂O (2 \times 25 mL), dried over Na_2SO_4 , filtered, and concentrated in vacuo. The crude material was purified by column chromatography.

2-(4-(3,4,5-Trimethoxyphenyl)-1H-pyrazol-3-yl)phenol (7): Purification by column chromatography (petroleum ether (PE)/EtOAc, 8:2 and 7:3) gave **7** as a yellow solid (130 mg, 80%): mp: 184–185 °C; 1H NMR (300 MHz, $CDCl_3$, 25 °C): δ = 10.90 (brs, 1 H), 7.64 (s, 1 H), 7.29 (d, J = 7.4 Hz, 1 H), 7.17 (t, J = 7.4 Hz, 1 H), 7.03 (d, J = 7.4 Hz, 1 H), 6.69 (t, J = 7.4 Hz, 1 H), 6.58 (s, 2 H), 3.91 (s, 3 H), 3.78 ppm (s, 6 H); ^{13}C NMR (75 MHz, $CDCl_3$, 25 °C): δ = 155.9, 153.4, 147.5, 137.4, 129.5, 129.3, 128.6, 120.8, 118.9, 117.1, 116.6, 115.8, 106.6, 61.1, 56.2 ppm; IR (KBr): $\tilde{\nu}$ = 3279, 2939, 1588, 1507, 1248, 1130, 998 cm^{-1} ; MS (ESI): m/z 327 [$M+H$]⁺; Anal. calcd for $C_{18}H_{18}N_2O_4$: C 66.25, H 5.56, N 8.58, found: C 66.20, H 5.58, N 8.50.

2-(4-(4-Methoxyphenyl)-1H-pyrazol-3-yl)phenol (8): Purification by column chromatography (PE/EtOAc, 7:3) gave **8** as a yellow solid (67 mg, 51%): mp: 123–124 °C (ref. [11] 118–119 °C); IR (KBr): $\tilde{\nu}$ = 3373, 1506, 1243, 1160 cm^{-1} ; MS (ESI): m/z 267 [$M+H$]⁺; Anal. calcd for $C_{16}H_{14}N_2O_2$: C 72.16, H 5.30, N 10.52, found: C 72.25, H 5.38, N 10.50.

2-(4-(2,3-Dihydrobenzo[b][1,4]dioxin-6-yl)-1H-pyrazol-3-yl)phenol (9):^[17] Purification by column chromatography (PE/EtOAc, 6:4) gave **9** as a light brown solid (67 mg, 46%): mp: 137–138 °C; 1H NMR (300 MHz, $CDCl_3$, 25 °C): δ = 10.44 (brs, 1 H), 7.55 (s, 1 H), 7.30 (dd, J = 7.7/1.4 Hz, 1 H), 7.25 (td, J = 7.7/1.4 Hz, 1 H), 7.02 (dd, J = 7.7/1.4 Hz, 1 H), 6.87–6.80 (m, 3 H), 6.70 (td, J = 7.7/1.4 Hz, 1 H), 4.28 ppm (s, 4 H); ^{13}C NMR (75 MHz, $CDCl_3$, 25 °C): δ = 155.7, 146.5, 143.6, 143.1, 140.0, 129.9, 129.3, 128.5, 126.4, 122.8, 120.2, 119.1, 118.2, 117.5, 117.0, 64.5 ppm (2C); IR (KBr): $\tilde{\nu}$ = 3403, 1583, 1522, 1498, 1282, 1246, 1160 cm^{-1} ; MS (ESI): m/z 295 [$M+H$]⁺; Anal. calcd for $C_{17}H_{14}N_2O_3$: C 69.38, H 4.79, N 9.52, found: C 69.31, H 4.70, N 9.52.

5-Methoxy-2-(4-(3,4,5-trimethoxyphenyl)-1H-pyrazol-3-yl)phenol (10): Purification by column chromatography (PE/EtOAc, 7:3) gave **10** as a light yellow solid (91 mg, 51%): mp: 201–202 °C; 1H NMR (300 MHz, $CDCl_3$, 25 °C): δ = 10.65 (brs, 1 H), 7.61 (s, 1 H), 7.19 (d, J = 8.5 Hz, 1 H), 6.58 (m, 3 H), 6.27 (dd, J = 8.5/2.1 Hz, 1 H), 3.90 (s, 3 H), 3.82 (s, 6 H), 3.77 ppm (s, 3 H); ^{13}C NMR (75 MHz, $[D_6]DMSO$, 25 °C): δ = 155.8, 151.6, 140.9, 139.8, 137.4, 130.4, 128.4, 120.5, 119.6, 117.5, 109.7, 103.6, 100.3, 59.0, 54.5, 54.0 ppm; IR (KBr): $\tilde{\nu}$ = 3268, 2988, 2840, 1632, 1589, 1265, 1130 cm^{-1} ; MS (ESI): m/z 357 [$M+H$]⁺; Anal. calcd for $C_{19}H_{20}N_2O_5$: C 64.04, H 5.66, N 7.86, found: C 64.12, H 5.67, N 7.95.

2-(4-(3-Hydroxy-4-methoxyphenyl)-1H-pyrazol-3-yl)-5-methoxyphenol (11): Purification by column chromatography (PE/EtOAc, 7:3) gave **11** as a white solid (103 mg, 66%): mp: 200–201 °C; 1H NMR (300 MHz, $CDCl_3$, 25 °C): δ = 7.55 (s, 1 H), 7.16 (d, J = 8.85 Hz, 1 H), 6.94 (s, 1 H), 6.84 (m, 2 H), 6.56 (s, 1 H), 6.24 (d, J = 8.5 Hz, 1 H), 3.93 (s, 3 H), 3.76 ppm (s, 3 H); ^{13}C NMR (75 MHz, $[D_6]DMSO$, 25 °C): δ = 160.7, 157.3, 146.8, 130.6, 130.1, 129.3, 128.5,

127.3, 119.4, 117.1, 117.0, 114.2, 112.8, 105.3, 102.0, 56.2, 55.5 ppm; IR (KBr): $\tilde{\nu}$ = 3359, 2834, 1623, 1511, 1283, 1226, 1198, 1071 cm^{-1} ; MS (ESI): m/z 313 $[M+H]^+$; Anal. calcd for $\text{C}_{17}\text{H}_{16}\text{N}_2\text{O}_4$: C 65.38, H 5.16, N 8.97, found: C 65.41, H 5.12, N 9.05.

5-Methoxy-2-(4-(4-methoxyphenyl)-1H-pyrazol-3-yl)phenol (12): Purification by column chromatography (PE/EtOAc, 7:3) gave **13** as a white solid (95 mg, 64%): mp: 204–205 °C (ref. [15a]) 150.5–151.6 °C; MS (ESI): m/z 297 $[M+H]^+$; Anal. calcd for $\text{C}_{17}\text{H}_{16}\text{N}_2\text{O}_5$: C 68.91, H 5.44, N 9.45, found: C 68.99, H 5.60, N 9.46.

2-(4-(2,3-Dihydrobenzo[b][1,4]dioxin-6-yl)-1H-pyrazol-3-yl)-5-methoxyphenol (13):^[18] Purification by column chromatography (PE/EtOAc, 8:2) gave **13** as a white solid (86 mg, 53%): mp: 122–123 °C; ¹H NMR (300 MHz, CDCl_3 , 25 °C): δ = 10.38 (brs, 1H), 7.54 (s, 1H), 7.19 (d, J = 8.8 Hz, 1H), 6.87–6.79 (m, 3H), 6.57 (s, 1H), 6.27 (d, J = 8.8 Hz, 1H), 4.28 (s, 4H), 3.77 ppm (s, 3H); ¹³C NMR (75 MHz, CDCl_3 , 25 °C): δ = 160.5, 157.3, 147.0, 143.6, 143.0, 129.4, 129.2, 126.4, 122.8, 119.7, 118.3, 117.5, 110.0, 105.8, 101.8, 64.5 (2C), 55.3 ppm; IR (KBr): $\tilde{\nu}$ = 3296, 2975, 1628, 1582, 1502, 1282, 1069 cm^{-1} ; MS (ESI): m/z 325 $[M+H]^+$; Anal. calcd for $\text{C}_{18}\text{H}_{16}\text{N}_2\text{O}_4$: C 66.66, H 4.97, N 8.64, found: C 66.73, H 5.01, N 8.61.

2-(4-(Benzo[d][1,3]dioxol-5-yl)-1H-pyrazol-3-yl)-5-methoxyphenol (14): Purification by column chromatography (PE/EtOAc, 8:2) gave **14** as a white solid (74 mg, 48%): mp: 161–162 °C; ¹H NMR (300 MHz, CDCl_3 , 25 °C): δ = 10.37 (brs, 1H), 7.54 (s, 1H), 7.15 (d, J = 8.5 Hz, 1H), 6.84–6.80 (m, 3H), 6.57 (d, J = 1.6 Hz, 1H), 6.28 (dd, J = 8.5/1.6 Hz, 1H), 5.99 (s, 2H), 3.77 ppm (s, 3H); ¹³C NMR (75 MHz, CDCl_3 , 25 °C): δ = 160.6, 157.4, 147.9, 146.5, 146.4, 129.4, 129.1, 126.8, 123.0, 119.9, 110.1, 109.9, 108.6, 105.8, 101.8, 101.2, 55.3 ppm; IR (KBr): $\tilde{\nu}$ = 3275, 1627, 1585, 1439, 1242, 1198, 1042 cm^{-1} ; MS (ESI): m/z 311 $[M+H]^+$; Anal. calcd for $\text{C}_{17}\text{H}_{14}\text{N}_2\text{O}_4$: C 65.80, H 4.55, N 9.03, found: C 65.94, H 4.61, N 9.09.

2,3-Dimethoxy-6-(4-(3,4,5-trimethoxyphenyl)-1H-pyrazol-3-yl)phenol (15): Purification by column chromatography (PE/EtOAc, 8:2) gave **15** as a white solid (129 mg, 67%): mp: 170–171 °C; ¹H NMR (300 MHz, CDCl_3 , 25 °C): δ = 9.24 (brs, 1H), 7.64 (s, 1H), 7.02 (d, J = 8.8 Hz, 1H), 6.58 (s, 2H), 6.32 (d, J = 8.8 Hz, 1H), 3.92 (s, 3H), 3.89 (s, 3H), 3.80 (s, 3H), 3.77 (s, 6H) 3.77 ppm (s, 3H); ¹³C NMR (75 MHz, CDCl_3 , 25 °C): δ = 153.8, 153.2, 150.5, 149.8, 136.9, 136.1, 130.6, 130.2, 129.9, 120.0, 119.7, 104.7, 103.7, 60.7, 60.6, 56.3, 56.0 ppm; IR (KBr): $\tilde{\nu}$ = 3416, 3053, 2940, 1580, 1431, 1121, 1091 cm^{-1} ; MS (ESI): m/z 387 $[M+H]^+$; Anal. calcd for $\text{C}_{20}\text{H}_{22}\text{N}_2\text{O}_6$: C 62.17, H 5.74, N 7.25, found: C 62.19, H 5.75, N 7.20.

6-(4-(3-Hydroxy-4-methoxyphenyl)-1H-pyrazol-3-yl)-2,3-dimethoxyphenol (16): Purification by column chromatography (PE/EtOAc, 6:4) gave **16** as a white solid (68 mg, 40%): mp: 185–186 °C; ¹H NMR (300 MHz, $[\text{D}_2\text{O}]\text{DMSO}$, 25 °C): δ = 8.84 (s, 1H), 7.58 (brs, 1H), 6.85–6.80 (m, 2H), 6.70–6.65 (m, 2H), 6.48 (d, J = 7.1 Hz, 1H), 3.77 (s, 3H), 3.73 (s, 3H), 3.69 ppm (s, 3H); IR (KBr): $\tilde{\nu}$ = 3408, 3050, 2955, 1581, 1420, 1127, 1090 cm^{-1} ; MS (ESI): m/z 343 $[M+H]^+$; Anal. calcd for $\text{C}_{18}\text{H}_{18}\text{N}_2\text{O}_5$: C 63.15, H 5.30, N 8.18, found: C 63.11, H 5.29, N 8.09.

2,3-Dimethoxy-6-(4-(4-methoxyphenyl)-1H-pyrazol-3-yl)phenol (17): Purification by column chromatography (PE/EtOAc, 7:3) gave **17** as a white solid (102 mg, 63%): mp: 193–194 °C; ¹H NMR (300 MHz, CDCl_3 , 25 °C): δ = 7.59 (s, 1H), 7.26 (d, J = 6.6 Hz, 2H), 6.94 (d, J = 6.6 Hz, 2H), 6.91 (d, J = 8.8 Hz, 1H), 6.30 ppm (d, J = 8.8 Hz, 1H); ¹³C NMR (75 MHz, CDCl_3 , 25 °C): δ = 158.8, 152.7, 149.1, 136.6, 130.5, 125.9, 123.6, 119.6, 114.1, 111.0, 103.3, 60.9, 55.9, 55.3 ppm; IR (KBr): $\tilde{\nu}$ = 3406, 2559, 1523, 1466, 1293, 1081 cm^{-1} ; MS

(ESI): m/z 327 $[M+H]^+$; Anal. calcd for $\text{C}_{18}\text{H}_{18}\text{N}_2\text{O}_4$: C 66.25, H 5.56, N 8.58, found: C 66.39, H 5.55, N 8.66.

6-(4-(2,3-Dihydrobenzo[b][1,4]dioxin-6-yl)-1H-pyrazol-3-yl)-2,3-dimethoxyphenol (18): Purification by column chromatography (PE/EtOAc, 6:4) gave **18** as a white solid (97 mg, 55%): mp: 176–177 °C; ¹H NMR (300 MHz, CDCl_3 , 25 °C): δ = 9.72 (brs, 1H), 7.57 (s, 1H), 7.01 (d, J = 8.8 Hz, 1H), 6.87–6.81 (m, 3H), 6.32 (d, J = 8.8 Hz, 1H), 4.27 (s, 4H), 3.92 (s, 3H), 3.83 ppm (s, 3H); ¹³C NMR (75 MHz, CDCl_3 , 25 °C): δ = 152.7, 149.0, 143.5, 142.8, 136.5, 126.9 (2C), 123.7, 122.6, 119.5, 118.0, 117.4 (2C), 110.9, 103.4, 64.5, 64.4, 60.9, 55.9 ppm; IR (KBr): $\tilde{\nu}$ = 3404, 2931, 1522, 1468, 1431, 1297, 1280, 1084 cm^{-1} ; MS (ESI): m/z 355 $[M+H]^+$; Anal. calcd for $\text{C}_{19}\text{H}_{18}\text{N}_2\text{O}_5$: C 64.40, H 5.12, N 7.91, found: C 64.56, H 5.22, N 7.98.

6-(4-(Benzo[d][1,3]dioxol-5-yl)-1H-pyrazol-3-yl)-2,3-dimethoxyphenol (19): Purification by column chromatography (PE/EtOAc, 7:3) gave **19** as a white solid (107 mg, 63%): mp: 174–175 °C; ¹H NMR (300 MHz, CDCl_3 , 25 °C): δ = 10.12 (brs, 1H), 7.57 (s, 1H), 6.97 (d, J = 9.0 Hz, 1H), 6.83–6.80 (m, 3H), 6.33 (d, J = 9.0 Hz, 1H), 5.97 (s, 2H), 3.92 (s, 3H), 3.83 ppm (s, 3H); ¹³C NMR (75 MHz, CDCl_3 , 25 °C): δ = 152.8, 149.1, 147.8, 146.8, 136.6, 132.2, 132.1, 128.8, 127.4, 123.6, 122.7, 110.9, 109.9, 108.5, 103.3, 101.1, 60.9, 55.9 ppm; IR (KBr): $\tilde{\nu}$ = 3386, 2953, 1607, 1465, 1435, 1233, 1080 cm^{-1} ; MS (ESI): m/z 341 $[M+H]^+$; Anal. calcd for $\text{C}_{18}\text{H}_{16}\text{N}_2\text{O}_5$: C 63.52, H 4.74, N 8.23, found: C 63.48, H 4.65, N 8.12.

2,3,4-Trimethoxy-6-(4-(3,4,5-trimethoxyphenyl)-1H-pyrazol-3-yl)phenol (20): Purification by column chromatography (PE/EtOAc, 7:3) gave **20** as an amorphous solid (93 mg, 45%): ¹H NMR (300 MHz, CDCl_3 , 25 °C): δ = 7.64 (s, 1H), 6.61 (s, 1H), 6.60 (s, 2H), 3.96 (s, 3H), 3.89 (s, 3H), 3.85 (s, 3H), 3.80 (s, 6H), 3.38 ppm (s, 3H); ¹³C NMR (75 MHz, CDCl_3 , 25 °C): δ = 153.3, 145.7, 143.5, 142.6, 141.7, 137.2, 129.4, 120.0, 118.5, 111.0, 106.9 (2C), 106.5, 61.3, 61.2, 61.0, 56.3, 55.7 ppm; IR (KBr): $\tilde{\nu}$ = 3300, 2937, 2833, 1583, 1463, 1238, 1126 cm^{-1} ; MS (ESI): m/z 417 $[M+H]^+$; Anal. calcd for $\text{C}_{21}\text{H}_{24}\text{N}_2\text{O}_7$: C 60.57, H 5.81, N 6.73, found: C 60.76, H 5.90, N 6.85.

6-(4-(3-Hydroxy-4-methoxyphenyl)-1H-pyrazol-3-yl)-2,3,4-trimethoxyphenol (21): Purification by column chromatography (PE/EtOAc, 7:3) gave **21** as a white solid (128 mg, 69%): mp: 224–225 °C; ¹H NMR (300 MHz, CDCl_3 , 25 °C): δ = 10.77 (brs, 1H), 7.42 (s, 1H), 6.83 (d, J = 1.4 Hz, 1H), 6.78–6.71 (m, 2H), 6.58 (s, 1H), 3.83 (s, 3H), 3.77 (s, 6H), 3.27 ppm (s, 3H); ¹³C NMR (75 MHz, CDCl_3 , 25 °C): δ = 146.7, 146.3, 144.9, 143.5, 142.3, 141.8, 126.9, 126.6, 120.9, 119.4, 116.8, 112.3, 112.0, 111.4, 106.4, 61.0, 60.8, 56.0, 55.6 ppm; IR (KBr): $\tilde{\nu}$ = 3398, 3276, 2934, 1560, 1507, 1463, 1429, 1255, 1071 cm^{-1} ; MS (ESI): m/z 373 $[M+H]^+$; Anal. calcd for $\text{C}_{19}\text{H}_{20}\text{N}_2\text{O}_6$: C 61.28, H 5.41, N 7.52, found: C 61.33, H 5.50, N 7.59.

2,3,4-Trimethoxy-6-(4-(4-methoxyphenyl)-1H-pyrazol-3-yl)phenol (22): Purification by column chromatography (PE/EtOAc, 7:3) gave **22** as a white solid (94 mg, 53%): mp: 158–159 °C; ¹H NMR (300 MHz, CDCl_3 , 25 °C): δ = 7.59 (s, 1H), 7.30 (d, J = 8.8 Hz, 2H), 6.93 (d, J = 8.8 Hz, 2H), 6.59 (s, 1H), 3.98 (s, 3H), 3.90 (s, 3H), 3.82 (s, 3H), 3.35 ppm (s, 3H); ¹³C NMR (75 MHz, CDCl_3 , 25 °C): δ = 159.0, 145.6, 143.2, 142.5, 141.7, 131.0, 130.5, 125.9, 119.8, 114.0, 111.2, 106.5, 105.1, 61.2 (2C), 55.7, 55.5 ppm; IR (KBr): $\tilde{\nu}$ = 3390, 2935, 2359, 1556, 1461, 1417, 1248, 1084 cm^{-1} ; MS (ESI): m/z 357 $[M+H]^+$; Anal. calcd for $\text{C}_{19}\text{H}_{20}\text{N}_2\text{O}_5$: C 64.04, H 5.66, N 7.86, found: C 63.99, H 5.65, N 7.87.

General procedure for the synthesis of intermediates 25a–c: A mixture of 3-methoxycatechol **23** (800 mg, 1.5 equiv), phenylacetic acid **24** (**24a** 858 mg, **24b** 692 mg, **24c** 632 mg, 1 equiv), *p*-T₂SOH (36 mg, 0.05 equiv), and $\text{BF}_3\cdot\text{Et}_2\text{O}$ (1 mL per mmol of **23**) was

heated at 85 °C for 90 min. The reaction mixture was poured into saturated aq. NaHCO₃, and the aqueous phase was extracted with EtOAc (2 × 50 mL). The combined organic phases were dried over Na₂SO₄ and evaporated, and the product was purified by crystallization from EtOH.

General procedure for the synthesis of intermediates 26a–c: Compound **25** (**25a** 433 mg, **25b** 367 mg, **25c** 350 mg, 1 equiv) was dissolved in dry toluene (2 mL), and *N,N*-dimethylformamide–dimethylacetate (DMF–DMA; 0.484 mL, 3 equiv) was added. The reaction mixture was heated at 90 °C for 30 min. The solvent was removed in vacuo to give a solid (**26a** 361 mg, **26b** 250 mg, **26c** 325 mg), which was used in the next step without further purification.

General procedure for the synthesis of pyrazoles 27–29: Compound **26** (**26a** 170 mg, **26b** 150 mg, **26c** 148 mg, 1 equiv) was dissolved in THF (4 mL). NH₂NH₂ solution (35% w/w in H₂O, 0.090 mL, 2 equiv) was added, and the reaction mixture was stirred at reflux for 3 h.

3-Methoxy-6-(4-(3,4,5-trimethoxyphenyl)-1H-pyrazol-3-yl)benzene-1,2-diol (27): Et₂O (39 mL) was added to the crude material (140 mg), and the resulting precipitate was filtered and washed with CH₂Cl₂ to give **27** as a white solid (117 mg, 63%): mp: 218–219 °C; ¹H NMR (300 MHz, CDCl₃, 25 °C): δ = 7.59 (s, 1H), 6.79 (d, *J* = 8.8 Hz, 1H), 6.57 (s, 2H), 6.30 (d, *J* = 8.8 Hz, 1H), 3.89 (s, 3H), 3.85 (s, 3H), 3.78 ppm (s, 6H); ¹³C NMR (75 MHz, CDCl₃, 25 °C): δ = 152.6, 146.3, 144.3, 134.0, 129.2, 119.0, 118.3, 118.0, 111.3, 105.6, 102.5, 60.3, 55.7, 55.6 ppm; IR (KBr): $\tilde{\nu}$ = 3487, 3332, 1589, 1430, 1238, 1132, 1078 cm⁻¹; MS (ESI): *m/z* 373 [M+H]⁺; Anal. calcd for C₁₉H₂₀N₂O₆: C 61.28, H 5.41, N 7.52, found: C 61.33, H 5.57, N 7.34.

3-(4-(3-Hydroxy-4-methoxyphenyl)-1H-pyrazol-3-yl)-6-methoxybenzene-1,2-diol (28): CH₂Cl₂ was added to the crude material, and the resulting precipitate was filtered to give **28** as a grey solid (83 mg, 51%): mp: 236–237 °C; ¹H NMR (300 MHz, [D₆]DMSO, 25 °C): δ = 8.25 (s, 1H), 7.65 (brs, 1H), 6.76 (d, *J* = 8.0 Hz, 1H), 6.65 (s, 1H), 6.60 (d, *J* = 8.0 Hz, 1H), 6.47 (d, *J* = 8.0 Hz, 1H), 6.35 (d, *J* = 8.0 Hz, 1H), 3.70 (s, 3H), 3.68 ppm (s, 3H); ¹³C NMR (75 MHz, [D₆]DMSO, 25 °C): δ = 148.8, 146.7, 145.3, 138.7, 134.6, 130.3, 128.9, 127.3, 121.2, 119.4, 118.7, 112.8, 111.8, 103.4, 101.2, 56.3, 56.2 ppm; IR (KBr): $\tilde{\nu}$ = 3438, 3320, 2584, 1528, 1505, 1443, 1291, 1079 cm⁻¹; MS (ESI): *m/z* 329 [M+H]⁺; Anal. calcd for C₁₇H₁₆N₂O₅: C 62.19, H 4.91, N 8.53, found: C 62.23, H 5.06, N 8.55.

3-Methoxy-6-(4-(4-methoxyphenyl)-1H-pyrazol-3-yl)benzene-1,2-diol (29): Purification by column chromatography (PE/EtOAc, 5:5) gave **29** as a yellow solid (82 mg, 53%): mp: 205–206 °C; ¹H NMR (300 MHz, CD₃OD, 25 °C): δ = 7.65 (s, 1H), 7.71 (d, *J* = 8.5 Hz, 2H), 6.83 (d, *J* = 8.5 Hz, 2H), 6.62 (d, *J* = 8.8 Hz, 1H), 6.38 (d, *J* = 8.8 Hz, 1H), 3.82 (s, 3H), 3.76 ppm (s, 3H); ¹³C NMR (75 MHz, CDCl₃, 25 °C): δ = 159.0, 145.2, 143.2, 142.5, 141.7, 134.5, 130.5, 127.5, 118.6, 114.3, 111.2, 106.5, 103.4, 56.2, 55.5 ppm; IR (KBr): $\tilde{\nu}$ = 3317, 2508, 1438, 1347, 1238, 1073 cm⁻¹; MS (ESI): *m/z* 313 [M+H]⁺; Anal. calcd for C₁₇H₁₆N₂O₄: C 65.38, H 5.16, N 8.97, found: C 65.49, H 5.22, N 9.03.

3-Methoxy-6-(1-methyl-4-(3,4,5-trimethoxyphenyl)-1H-pyrazol-3-yl)benzene-1,2-diol (30): Compound **26a** (150 mg, 0.44 mmol) was dissolved in THF (4 mL). *N*-Methylhydrazine solution (35% w/w in H₂O, 134 μL, 2 equiv) was added to the reaction mixture. After 3 h at reflux, the volatile material was evaporated, and the residue was diluted with EtOAc/H₂O. The organic layer was washed with H₂O (2 × 25 mL), dried over Na₂SO₄, and concentrated in vacuo. Purification by column chromatography (PE/EtOAc, 4:6) gave **30** as

a white solid (85 mg, 50%): mp: 143–145 °C; ¹H NMR (300 MHz, CDCl₃, 25 °C): δ = 10.86 (brs, 1H), 7.36 (s, 1H), 6.77 (d, *J* = 8.8 Hz, 1H), 6.53 (s, 2H), 6.26 (d, *J* = 8.8 Hz, 1H), 3.93 (s, 3H), 3.88 (s, 3H), 3.82 (s, 3H), 3.76 ppm (s, 6H); ¹³C NMR (75 MHz, [D₆]DMSO, 25 °C): δ = 153.1, 148.6, 146.2, 145.2, 136.3, 134.5, 130.7, 129.4, 120.5, 120.0, 114.3, 105.1, 103.3, 60.5, 56.3, 56.0, 39.3 ppm; IR (KBr): $\tilde{\nu}$ = 3357, 2932, 1586, 1518, 1288, 1128, 1091 cm⁻¹; MS (ESI): *m/z* 387 [M+H]⁺; Anal. calcd for C₂₀H₂₂N₂O₆: C 62.17, H 5.74, N 7.25, found: C 62.31, H 5.70, N 7.23.

3-Methoxy-6-(4-(3,4,5-trimethoxyphenyl)isoxazol-5-yl)benzene-1,2-diol (31): Compound **26a** (100 mg, 0.29 mmol) was dissolved in EtOH (2 mL) and pyridine (0.5 mL). NH₂OH·HCl (20 mg, 2 equiv) was added, and the reaction was stirred at 65 °C for 2 h. The volatile material was evaporated, and the reaction was diluted with EtOAc and washed with 2 M HCl (2 × 25 mL). The organic phase was dried over Na₂SO₄ and evaporated. The crude product was purified by column chromatography (PE/EtOAc, 6:4) to give **31** as a brown amorphous solid (70 mg, 64%): ¹H NMR (300 MHz, CDCl₃, 25 °C): δ = 8.43 (s, 1H), 6.92 (d, *J* = 8.8 Hz, 1H), 6.54–6.51 (m, 3H), 3.90 (s, 3H), 3.84 (s, 3H), 3.73 ppm (s, 6H); ¹³C NMR (75 MHz, CDCl₃, 25 °C): δ = 162.3, 153.5, 150.8, 148.8, 142.5, 137.7, 133.4, 125.5, 121.1, 117.0, 108.5, 105.0, 103.6, 61.0, 56.3, 56.1 ppm; IR (KBr): $\tilde{\nu}$ = 3485, 3330, 1600, 1425, 1237, 1130, 1075 cm⁻¹; MS (ESI): *m/z* 374 [M+H]⁺; Anal. calcd for C₁₉H₁₉NO₇: C 61.12, H 5.13, N 3.75, found: C 61.23, H 5.20, N 3.81.

Biological evaluation

Cell culture and cytotoxicity assay: The SH-SY5Y human neuroblastoma cell line was obtained from ATCC (LGC Promochem Teddington, UK) and cultured in 50% MEM and 50% F-12 supplemented with 10% fetal bovine serum, 2 mM glutamine, 100 μg mL⁻¹ penicillin, and 100 μg mL⁻¹ streptomycin. The epithelioid malignant pleural mesothelioma-derived REN cell line was kindly provided by Dr. S. M. Albelda (University of Pennsylvania, Philadelphia, PA), and the MSTO-211H cell line, established from the pleural effusion of a patient with biphasic mesothelioma of the lung, was obtained from the Istituto Scientifico Tumori (IST) Cell Bank (Genoa, Italy); cells were cultured in RPMI medium supplemented with 10% fetal bovine serum (FBS) at 37 °C in a 5% CO₂-humidified atmosphere. For cytotoxicity assays, cells were plated on 24-well plates and grown for 64 h (for the screening phase) or 48 h in the presence or absence of combretastatin A4 (**1**), combretastatin A1 (**3**), or the synthesized compounds. On the experimental day, cells were incubated for 1 h with MTT (250 μg mL⁻¹ in Locke's solution) at 37 °C. Reactions were then stopped, and the crystals were solubilized in *i*PrOH/HCl before reading at 570 nm in a spectrophotometer. To determine IC₅₀ values, data were plotted and fitted using GraphPad Prism software (San Diego, CA, USA).

Tubulin polymerization assay: To measure the degree of tubulin polymerization, we used a reported method.^[19] Briefly, SH-SY5Y cells were grown in 57 cm² dishes in the presence or absence of drugs for 24 h. Cells were then trypsinized and centrifuged twice at 600 *g* for 5 min. Cells were then resuspended in 70 μL of hypotonic buffer (20 mM Tris-HCl pH 6.8, 1 mM MgCl₂, 2 mM EGTA, Sigma Protease Inhibitor Cocktail (P8340), and 0.5% Igepal) containing 4 μg mL⁻¹ paclitaxel. Lysates were incubated for 10 min at room temperature and then vortexed. Lysates were then centrifuged at 13 000 rpm for 15 min at room temperature. The supernatant and pellet were then resuspended in equal volumes of SDS loading buffer and run on a 10% SDS-PAGE polyacrylamide gel. After transfer of proteins to nitrocellulose (blocked in 5% milk), tu-

bulin was identified with an anti-tubulin primary antibody (1:1000, Sigma–Aldrich) and an anti-mouse peroxidase-conjugated secondary antibody (1:8000, Amersham Bioscience) and were visualized by chemiluminescence (Supersignal WestPico, Pierce).

Flow cytometric analysis of cell-cycle status: Cells grown in the presence or absence of compounds for 24 h were washed once in PBS and resuspended in 1 mL of ice-cold PBS/EtOH (30:70) and stored at -20°C . Cells were then washed twice in PBS and resuspended in PBS containing RNase ($100\ \mu\text{g mL}^{-1}$) for 1 h at 37°C . DNA was then stained with a PBS solution containing 5 mM EDTA and $100\ \mu\text{g mL}^{-1}$ propidium iodide. Cell-cycle analysis was determined using a FACS Vantage SE DiVa (Becton Dickinson, San Jose, CA, USA).

In vitro metabolism: The procedure used to investigate in vitro metabolism is detailed in the Supporting Information.

Molecular modeling

All molecular modeling studies were performed on a Tesla workstation equipped with two Intel Xenon Processors (X5650 2.67 GHz and Ubuntu 10.04). Different crystal structures of colchicine domain inhibitors have been reported; in our study, the X-ray structure of the α,β -tubulin–E7010 complex was used (PDB ID: 3HKC).^[29] The stathmin-like domain, subunits C and D, E7010, and water molecules were removed; the binding site was detected using the original ligand coordinates. Ligand structures were built from a SMILES string and were minimized using Omega2.^[30] As a standard of comparison, CA1 was docked together with the analogues. The docking simulations were performed using FRED, and default settings were used.^[31] All structural images were prepared using PyMOL.^[32]

Acknowledgements

Financial support from the Italian Ministry of Education, Universities and Research (MIUR)–Projects of National Interest (PRIN) Initiative (2008) is gratefully acknowledged. The authors also acknowledge the gift of REN and MSTO-211H cells from Prof. Laura Moro (University of Piemonte Orientale, Novara, Italy). A.M. and G.S. gratefully acknowledge OpenEye Scientific Software Inc. for providing an academic license for their software packages.

Keywords: antitumor agents • cytotoxicity • combretastatins • multicomponent reactions • tubulin • vascular disrupting agents

- [1] a) P. E. Thorpe, *Clin. Cancer Res.* **2004**, *10*, 415–427; b) D. W. Siemann, D. J. Chaplin, M. R. Horsman, *Cancer* **2004**, *100*, 2491–2499; c) G. M. Tozer, C. Kanthou, B. C. Baguley, *Nat. Rev. Cancer* **2005**, *5*, 423–435; d) M. J. McKeage, B. C. Baguley, *Cancer* **2010**, *116*, 1859–1871.
- [2] G. R. Pettit, S. B. Singh, E. Hamel, C. M. Lin, D. S. Alberts, D. Garcia-Kendall, *Experientia* **1989**, *45*, 209–211.
- [3] a) C. Kanthou, G. M. Tozer, *Int. J. Exp. Pathol.* **2009**, *90*, 284–294; b) C. Dumontet, M. A. Jordan, *Nat. Rev. Drug Discovery* **2010**, *9*, 790–803.
- [4] C. M. Lin, H. H. Ho, G. R. Pettit, E. Hamel, *Biochemistry* **1989**, *28*, 6984–6991.
- [5] a) S. L. Young, D. J. Chaplin, *Expert Opin. Invest. Drugs* **2004**, *13*, 1171–1182; b) <http://www.clinicaltrials.gov> NCT00507429, NCT00653939, NCT00113438, NCT00060242, NCT00395434.
- [6] a) D. M. Patterson, M. Zweifel, M. R. Middleton, P. M. Price, L. K. Folkes, M. R. Stratford, P. Ross, S. Halford, J. Peters, J. Balkissoon, D. J. Chaplin, A. R. Padhani, G. J. Rustin, *Clin. Cancer Res.* **2012**, *18*, 1415–1425; b) <http://www.clinicaltrials.gov> NCT0097210, NCT00960557.
- [7] a) S. A. Hill, G. M. Toze, G. R. Pettit, D. J. Chaplin, *Anticancer Res.* **2002**, *22*, 1453–1458; b) H. W. Salmon, D. W. Siemann, *Clin. Cancer Res.* **2006**, *12*, 4090–4094.
- [8] J. Y. Hua, Y. Sheng, K. G. Pinney, C. M. Garner, R. R. Kane, J. A. Prezioso, G. R. Pettit, D. J. Chaplin, K. Edvardsen, *Anticancer Res.* **2003**, *23*, 1433–1440.
- [9] a) L. K. Folkes, M. Christlieb, E. Madej, M. R. Stratford, P. Wardman, *Chem. Res. Toxicol.* **2007**, *20*, 1885–1894; b) G. R. Pettit, A. J. Thornhill, B. R. Moser, F. Hogan, *J. Nat. Prod.* **2008**, *71*, 1561–1563; c) L. Rice, C. Pampo, S. Lepler, A. M. Rojiani, D. W. Siemann, *Microvasc. Res.* **2011**, *81*, 44–51; d) J. W. Lippert, *Bioorg. Med. Chem.* **2007**, *15*, 605–615.
- [10] a) N. H. Nam, *Curr. Med. Chem.* **2003**, *10*, 1697–1722; b) G. C. Tron, T. Pirali, G. Sorba, F. Pagliai, S. Busacca, A. A. Genazzani, *J. Med. Chem.* **2006**, *49*, 3033–3044. The trimethoxybenzene moiety is not crucial for all the analogues of combretastatin. Some authors have recently highlighted that in the case of 4-arylcoumarin compounds, the trimethoxy groups in ring A are not essential for antiproliferative activity: S. Combes, P. Barbier, S. Douillard, A. McLeer-Florin, V. Bourgarel-Rey, J.-T. Pierson, A. Y. Fedorov, J.-P. Finet, J. Boutonnat, V. Peyrot, *J. Med. Chem.* **2011**, *54*, 3153–3162.
- [11] F. Xie, G. Cheng, Y. Hu, *J. Comb. Chem.* **2006**, *8*, 286–288.
- [12] R. LeBlanc, J. Dickson, T. Brown, M. Stewart, H. N. Pati, D. VanDerveer, H. Arman, J. Harris, W. Pennington, H. L. Holt, M. Lee, *Bioorg. Med. Chem.* **2005**, *13*, 6025–6034.
- [13] K. Ohsumi, T. Hatanaka, K. Fujiita, R. Nakagawa, Y. Fukuda, Y. Nihei, Y. Suga, Y. Morinaga, Y. Akiyama, T. Tsuji, *Bioorg. Med. Chem. Lett.* **1998**, *8*, 3153–3158.
- [14] I. Yokoe, Y. Sugita, Y. Shirataki, *Chem. Pharm. Bull.* **1989**, *37*, 529–530.
- [15] a) Z.-T. Zhang, D.-J. Tan, D. Xue, *Helv. Chim. Acta* **2007**, *90*, 2096–2108; b) V. P. Khilya, A. Aitmambetov, M. Ismailov, L. G. Grishko, *Chem. Nat. Compd.* **1994**, *30*, 580–583.
- [16] a) R. B. Gammill, *Synthesis* **1979**, 901–903; b) D. A. Vasselin, A. D. Westwell, C. S. Matthews, T. D. Bradshaw, M. F. Stevens, *J. Med. Chem.* **2006**, *49*, 3973–3981; c) A. Matin, N. Gavande, M. S. Kim, N. X. Yang, N. K. Salam, J. R. Hanrahan, R. H. Roubin, D. E. Hibbs, *J. Med. Chem.* **2009**, *52*, 6835–6850; d) N. Gavande, N. Karim, G. A. R. Johnston, J. R. Hanrahan, M. Chebib, *ChemMedChem* **2011**, *6*, 1340–1346.
- [17] J. M. Sheridan, J. R. Heal, W. D. O. Hamilton, I. Pike, (Electrophoretics Ltd., Cobham, UK), PCT Int. Appl. WO2012/080729A2, **2012**; [*Chem. Abstr.* **2012**, *157*, 122958].
- [18] M. J. Drysdale, B. W. Dymock, X. Barril-Alonso, P. Workman, L. H. Pearl, C. Prodromou, E. MacDonald, (Ribotargets Ltd., Abington, UK; Cancer Research Technology, London, UK; Institute of Cancer Research, London, UK), PCT Int. Appl. WO2003/055860A1, **2003**; [*Chem. Abstr.* **2012**, *139*, 101122].
- [19] T. Pirali, S. Busacca, L. Beltrami, D. Imovilli, F. Pagliai, G. Miglio, A. Marsarotti, L. Verotta, G. C. Tron, G. Sorba, A. A. Genazzani, *J. Med. Chem.* **2006**, *49*, 5372–5376.
- [20] a) B. L. Flynn, G. S. Gill, D. W. Grobelny, J. H. Chaplin, D. Paul, A. F. Leske, T. C. Lavranos, D. K. Chalmers, S. A. Charman, E. Kostewicz, D. M. Shackelford, J. Morizzi, E. Hamel, M. K. Jung, G. Kremmidiotis, *J. Med. Chem.* **2011**, *54*, 6014–6027; b) A. F. Leske, D. C. Bibby, T. C. Lavranos, D. Beaumont, J. Gasic, D. Rischin, J. Desai, G. Chong, S. S. Wong, B. Flynn, G. Kremmidiotis, “Discovery and Clinical Development of BNC105, a Tubulin-Targeting Small Molecule That Selectively Disrupts the Vasculature in Solid Tumours”, Poster, 23rd Lorne Cancer Conference, **2011**, <http://cdn.f1000.com/posters/docs/863>.
- [21] B. W. Robinson, A. W. Musk, R. A. Lake, *Lancet* **2005**, *366*, 397–408.
- [22] W. R. Smythe, L. R. Kaiser, H. C. Hwang, K. M. Amin, J. M. Pilewski, S. J. Eck, J. M. Wilson, S. M. Albelda, *Ann. Thorac. Surg.* **1994**, *57*, 1395–1401.
- [23] G. Bepeler, A. Koehler, P. Kiefer, K. Havemann, K. Beisenherz, G. Jaques, C. Gropp, M. Haeder, *Differentiation* **1988**, *37*, 158–171.
- [24] C.-M. Sun, L.-G. Lin, H.-J. Yu, C.-Y. Tsai, Y.-C. Chu, Y.-H. Din, Y.-P. Chau, M.-J. Don, *Bioorg. Med. Chem. Lett.* **2007**, *17*, 1078–1081.
- [25] K. Sugihara, S. Kitamura, K. Tatsumi, *Drug Metab. Dispos.* **1996**, *24*, 199–202.
- [26] a) S. Aprile, E. Del Grosso, G. Grosa, *Xenobiotica* **2009**, *39*, 148–161; b) M. R. Stratford, L. K. Folkes, *J. Pharm. Biomed. Anal.* **2012**, *62*, 114–118.

- [27] D. B. Kitchen, H. Decornez, J. R. Furr, J. Bajorath, *Nat. Rev. Drug Discovery* **2004**, *3*, 935–949.
- [28] A. Massarotti, A. Coluccia, R. Silvestri, G. Sorba, A. Brancale, *ChemMedChem* **2012**, *7*, 33–42.
- [29] A. Dorléans, B. Gigant, R. B. Ravelli, P. Mailliet, V. Mikol, M. Knossow, *Proc. Natl. Acad. Sci. USA* **2009**, *106*, 13775–13779.
- [30] Omega2, version 2.4.6, OpenEye Scientific Software, **2012**.
- [31] M. McGann, *J. Comput.-Aided Mol. Design* **2012**, *26*, 897–906.
- [32] The PyMOL Molecular Graphics System, version 1.3, Schrödinger LLC, **2010**.

Received: December 4, 2012

Revised: January 23, 2013

Published online on February 21, 2013